IVYSPRING INTERNATIONAL PUBLISHER

Theranostics

2019; 9(15): 4437-4449. doi: 10.7150/thno.34953

Research Paper

Novel ginsenoside-based multifunctional liposomal delivery system for combination therapy of gastric cancer

Chao Hong[1#], Dan Wang[1,2#], Jianming Liang[1,3], Yizhen Guo[1], Ying Zhu[4], Jiaxuan Xia[1], Jing Qin[1], Huaxing Zhan[2], Jianxin Wang[1,5]✉

1. Department of Pharmaceutics, School of Pharmacy, Fudan University & Key Laboratory of Smart Drug Delivery, Ministry of Education, Shanghai 201203, China
2. Shanghai Ginposome Pharmatech Co., Ltd, Shanghai 201600, China
3. Institute of Tropical Medicine, Guangzhou University of Chinese Medicine, Guangzhou 510006, China
4. Institute of Clinical Pharmacology, Guangzhou University of Traditional Chinese Medicine, Guangzhou 510006, China
5. Institute of Integrated Chinese and Western Medicine, Fudan University, Shanghai 200040, China

#Chao Hong and Dan Wang contributed equally to this work

✉ Corresponding author: Jianxin Wang, Tel.: 86-21-51980088; Fax: 86-21-51980088; E-mail: jxwang@fudan.edu.cn

Received: 2019.03.17; Accepted: 2019.05.20; Published: 2019.06.09

Abstract

The clinical treatment of gastric cancer (GC) is hampered by the development of anticancer drug resistance and the unfavorable pharmacokinetics, off-target toxicity, and inadequate intratumoral accumulation of the current chemotherapy treatments. Ginsenosides combined with paclitaxel (PTX) have been shown to exert synergistic inhibition of human GC cell proliferation. In the present study, we developed a novel multifunctional liposome system, in which ginsenosides functioned as the chemotherapy adjuvant and membrane stabilizer. These had long blood circulation times and active targeting abilities, thus creating multifunctionality of the liposomes and facilitating drug administration to the GC cells.

Methods: Three ginsenosides with different structures were used to formulate the unique nanocarrier, which was prepared using the thin-film hydration method. The stability of the ginsenoside liposomes was determined by particle size analysis using dynamic light scattering. The long circulation time of ginsenoside liposomes was compared with that of conventional liposome and polyethylene glycosylated liposomes *in vivo*. The active targeting effect of ginsenoside liposomes was examined with a GC xenograft model using an *in vivo* imaging system. To examine the antitumor activity of ginsenoside liposomes against GC, MTT, cell cycle, and apoptosis assays were performed on BGC-823 cells *in vitro* and PTX-loaded ginsenoside liposomes were prepared to evaluate the therapeutic efficacy on GC *in vivo*.

Results: The ginsenosides stabilized the liposomes in a manner similar to cholesterol. We confirmed the successful delivery of the bioactive combination drugs and internalization into GC cells via analysis of the glucose-related transporter recognition and longer blood circulation time. PTX was encapsulated in different liposomal formulations for use as a combination therapy, in which ginsenosides were found to exert their inherent anticancer activity, as well as act synergistically with PTX. The combination therapy using these targeted liposomes significantly suppressed GC tumor growth and outperformed most reported PTX formulations, including Lipusu® and Abraxane®.

Conclusion: We established novel ginsenoside-based liposomes as a tumor-targeting therapy, in which ginsenoside functioned not only as a chemotherapy adjuvant, but also as a functional membrane material. Ginsenoside-based liposomes offer a novel platform for anticancer drug delivery and may lead to a new era of nanocarrier treatments for cancer.

Key words: Ginsenoside; liposome; multifunction; gastric cancer; combination therapy; paclitaxel.

Introduction

Gastric cancer (GC) is one of the most frequently occurring cancers worldwide and is a leading cause of cancer-related deaths. The initial detection of most GC cases occurs at an advanced stage because the early stages are clinically silent [1]. Although advances have been made toward understanding the biology of GC, the available treatments for patients with advanced GC remain unsatisfactory. Currently, the major therapeutic strategies for patients with GC include surgery, chemotherapy, and radiotherapy. Although chemotherapy is the preferred option [2], the treatment efficacy is hampered by the development of drug resistance as well as unfavorable pharmacokinetics and inadequate intratumoral accumulation of the current therapeutic agents [3].

Many studies have suggested that the administration of herb–drug combinations could significantly alleviate drug resistance and enhance the response of patients with GC to chemotherapy [4-9]. Among the various herbs proposed to improve cancer treatment, ginseng has attracted the most interest worldwide. Numerous studies have shown that ginseng is able to treat cancer-related symptoms and has the potential to improve the quality of life of patients with cancer [10-12]. Among the various components of ginseng, ginsenosides have been identified as the main active components and have been investigated extensively [13]. The powerful antitumor activities of ginsenosides have been demonstrated both *in vitro* and *in vivo*, and inhibit the development, angiogenesis, and metastasis of tumors [14-17]. Ginsenosides can improve therapeutic efficacy and decrease the adverse reactions to many anticancer drugs, including doxorubicin, paclitaxel (PTX), cisplatin, and mitomycin [18-20]. For example, the co-treatment of ginsenoside Rg3 with mitomycin C and tegafur in patients with advanced GC after surgical resection resulted in lower angiogenesis and improved survival rates [21].

It has been reported that, when used in combination therapies, the pharmacokinetic profiles of each individual drug in the blood may be altered, leading to the distinct biodistribution of each component [22, 23]. Ginsenosides are readily degradable in the gastrointestinal tract and blood; therefore, they might not reach the tumor site concurrently with the anticancer agents, which greatly reduces their synergistic effects [13]. Fortunately, nanoparticle-based drug delivery vehicles provide a platform for the co-delivery of multiple anticancer drugs to the same site, allowing strong synergistic antitumor effects to be achieved. Among the numerous nanocarriers that have been utilized for drug delivery, liposomes are the most promising and widely accepted because of their non-toxic and non-immunogenic characteristics, and high loading capacity for drugs that have different physicochemical properties [24]. Therefore, the use of a liposomal carrier to achieve the co-delivery of ginsenoside and a chemotherapy agent represents an optimal choice that could result in enhanced therapeutic efficacy and reduced off-target toxicity. Unlike conventional liposomes, to improve the tumor-selective drug deposition we used ginsenoside as a multifunctional membrane material to stabilize the structure and enhance the accumulation of liposomes at the tumor site. Ginsenosides have a similar steroid structure to cholesterol (Figure 1A); therefore, researchers have used different technologies to study the interaction among ginsenosides with various phospholipids and have shown that ginsenosides can potentially stabilize the phospholipid bilayer, similar to that of cholesterol [25, 26]. The insertion of ginsenoside would therefore lead to a different lipid packing order, size, and surface status of the phospholipid bilayer in liposomes, which may influence their *in vivo* fate. In addition, ginsenosides are confirmed substrates of glucose-related transporters that are overexpressed in certain tumors, including GC [27]. For example, both *in vitro* and *in vivo* studies have shown that the transport of ginsenoside Rb1 across the blood-brain barrier was mediated by glucose transporter 1 (GLUT1) [28]. Similarly, a previous study revealed that ginsenoside Rg1 was actively transported via sodium-coupled glucose co-transporter 1 (SGLT1) into the intestine [29]. Thus, ginsenoside has the potential to work as an active targeting ligand to facilitate the accumulation of drug-loading liposomes at the tumor site via interaction with the GLUT of tumor cells.

Owing to the established anticancer activities and physicochemical properties of ginsenosides, we developed novel ginsenoside-based liposomes for tumor-targeting therapy, in which ginsenoside functioned as not only the chemotherapy adjuvant, but also the functional membrane material to stabilize the lipid bilayer structure, prolong blood circulation, and actively target cancer cells. Three ginsenosides that are commonly used in cancer therapy, Rh2, Rg3, and Rg5, were optimized in the present study. The biggest difference between ginsenoside and cholesterol is the additional glycoside chains, which significantly change their physicochemical properties (Figure 1A) [13]. The addition of the hydrophilic glycoside chains significantly decreases the lipophilicity of ginsenosides compared to cholesterol (logP of cholesterol, Rh2, Rg3, and Rg5 are 9.619 ± 0.281, 5.025 ± 0.428, 5.140 ± 0.854, and 6.934 ± 0.858,

respectively; data from SciFinder). In addition, ginsenoside Rg3 has been developed as a class I new drug in traditional Chinese medicine (Shenyi capsule) and is used clinically in China for the treatment of various types of cancer, including lung and breast cancers, and gastrointestinal tumors [14, 19, 21], which is distinct from the almost ineffective cholesterol. However, recent studies have shown that ginsenoside Rh2 exhibited stronger antitumor activities than that of Rg3, and has one less sugar moiety (at the C-3 position) than Rg3 [16, 18]. Another ginsenoside, Rg5, is the product of the dihydroxylation of Rg3 at C-20 and has shown much weaker antitumor efficacy [13, 17]. Therefore, three unique liposomes have been manufactured using these three ginsenosides that have different structures and antitumor effects [30-32]. We evaluated the delivery and internalization of ginsenoside liposomes into GC cells via their circulation in the blood and GLUT recognition, and determined the resulting inhibition of cell proliferation via cell-cycle analysis and apoptosis induction. Finally, we encapsulated PTX in different liposomal formulations for use as a combination therapy, in which ginsenosides exerted not only their inherent anticancer activity, but also exhibited a prominent synergistic effect with PTX, resulting in anti-GC activity.

Methods

Materials

Egg yolk lecithin (EYPC) was purchased from A.V. T. Pharmaceutical Co., Ltd (Shanghai, China). Cholesterol was purchased from Sinopharm Chemical Reagent Co., Ltd (Shanghai, China) and PTX was obtained from Dalian Meilun Biotechnology Co., Ltd (Dalian, China). Soybean oil; Lipusu® (paclitaxel liposome for injection); Abraxane® (paclitaxel protein-bound particles for injectable suspension); and ginsenosides Rh2, Rg3, and Rg5 were provided by Shanghai Ginposome Pharmatech Co. Ltd. (Shanghai, China). 5-(Dimethyl-thiazol-2-yl)-2,5-diphenyl-tetrazolium bromide (MTT) was purchased from Sigma (St. Louis, MO, USA). Hoechst 333425, 4-chlorobenzenesulfonate salt (DID), 1,1'-dioctadecyl-3,3,3',3'-tetramethylindotricarbocyanineiodide (DIR), and carboxyfluorescein (FAM) were obtained from Fanbo Biochemicals (Beijing, China). N-(Carbonyl-methoxypolyethylene glycol 2000)-1,2-distearoyl-sn-glycero-3-phosphoethanolamine was obtained from NOF Co. (Tokyo, Japan).

Preparation and characterization of liposomes

Liposomes were prepared by the thin-film hydration method. Conventional liposomes were prepared with a formulation of EYPC:cholesterol in a 10:3 mass ratio, and ginsenoside Rh2 liposome (Rh2-lipo) was prepared with the same lipid composition (EYPC:Rh2; 10:3 mass ratio). Ginsenoside Rg3 liposome (Rg3-lipo) was prepared with EYPC:Rg3 in a 5:2 mass ratio, and ginsenoside Rg5 liposome (Rg5-lipo) with EYPC:Rg5:soybean oil in a 10:4:5 mass ratio. First, all lipid materials were dissolved in 1 mL chloroform ($CHCl_3$) and ethyl alcohol (CH_3CH_2OH) (1:1 volume ratio). A rotary evaporator (ZX-98; LOOYE, China) was used to form a lipid film at 50 °C. After the thin film was hydrated with 1 mL 5% glucose solution at 50 °C for 30 min, the liposomal suspension was subjected to a probing sonication process (5 s sonication followed by 5 s rest) in an ice bath for 5 min at 300 W (20 kHz; Sonics & Materials, Inc.). PTX-loaded liposomes were prepared by the same method as that described previously for EYPC:PTX with a mass ratio of 15:1.

The particle size and ζ-potential of all liposomes were detected by a dynamic light scattering (DLS) detector (Zetasizer, Nano-ZS; Malvern, UK). The encapsulation efficiency (EE) and loading efficiency (LE) of PTX were measured following the methodology described in a previous study [33].

Stability of liposomes

To evaluate the stability of the ginsenoside liposomes, changes in size were observed by DLS over 1 week at 4 °C.

The stability of PTX-loaded liposomes in PBS was determined at 4 °C for 1 week and 37 °C for 48 h. To further determine the stability in blood, PTX-loaded liposomes were incubated with 10% fetal bovine serum (FBS; Gibco, USA), and changes in the average size and polydispersity index (PDI) were measured by DLS for 48 h.

PTX leakage from the liposomes was also monitored for 48 h at 37 °C to determine the EE. Each sample had three replications.

Pharmacokinetics study

To illustrate the blood circulation of the ginsenoside liposomes, the pharmacokinetics of the drug were determined in ICR mice (bodyweight 18–22 g) following the methodology described by a previous study [34]. One aliquot each of 200 μL DID-loaded cholesterol liposome (C-lipo), polyethylene glycolated C-lipo (PEG-C-lipo), Rh2-lipo, Rg3-lipo, and Rg5-lipo was injected into the mice via the tail vein. A 50 μL blood sample was collected by cheek pouch puncture at 2, 5, 15, and 30 min, and 1, 3, 6, 12, and 24 h after drug administration. The collected blood samples were diluted with 50 μL of 1× PBS in a 96-well plate and measured using a fluorescence spectrometer (640/670

nm). PEG-C-lipo was prepared using the same method as that described previously, with PEG:EYPC:cholesterol in a mass ratio of 2:10:3. DID-loaded liposomes were prepared with EYPC:DID in a 1000:1 mass ratio. Each sample had three replications.

In vitro cellular uptake

To evaluate the targeting ability of the ginsenoside liposomes, BGC-823 cells were seeded at a density of 2 × 10^5 cells/well in 12-well plates. After 12 h, the cells were incubated with FAM-loaded C-lipo, Rh2-lipo, Rg3-lipo, and Rg5-lipo at a final FAM concentration of 500 ng/mL at 37 °C. After incubation for 4 h, the cells were stained with Hoechst 33342 and then washed three times with cold PBS. Finally, the samples were visualized using a confocal microscope (Carl Zeiss, Germany). For the quantitative study, BGC-823 cells treated with FAM-loaded liposomes were collected, digested, and analyzed using a flow cytometer (FACS Calibur; BD Biosciences, USA).

To study the uptake mechanism, BGC-823 cells were pre-incubated with 20 mM glucose, 0.3 mM phloridzin, or 0.2 mM quercetin for 60 min [35-37], and then analyzed using the procedure described previously.

In vivo animal imaging

The *in vivo* tumor-targeting effect of the ginsenoside liposomes was determined in nude mice subcutaneously injected with the model tumor (BGC-823 cells). When the volume of the tumor reached approximately 100 mm^3, the mice were randomly divided into four groups and injected via the tail vein with DiR-loaded C-lipo, Rh2-lipo, Rg3-lipo, and Rg5-lipo. The fluorescence distribution was determined using an *in vivo* imaging system (IVIS Spectrum; Caliper, USA) at predetermined time points (2, 4, 8, 12, and 24 h). After 24 h, the mice were sacrificed by heart perfusion with saline, and the tumors were collected and imaged.

Cytotoxicity assay

The MTT assay was used to determine the toxicity of ginsenoside liposomes and PTX-loaded ginsenoside liposomes to BGC-823 cells. Briefly, BGC-823 cells were seeded in 96-well plates at a density of 3 × 10^3 cells/well, and treated with various concentrations of free PTX, PTX-C-lipo, PTX-Rh2-lipo, PTX-Rg3-lipo, PTX-Rg5-lipo, PTX+Rh2-lipo, PTX+Rg3-lipo, PTX+Rg5-lipo, Rh2-lipo, Rg3-lipo, Rg5-lipo, Rh2, Rg3, and Rg5 for 48 h; an equal concentration of each PTX-loaded ginsenoside liposome was used. Subsequently, the MTT assay was followed in accordance with the manufacturer's protocol. The cell viability was calculated from the following equation:

$$Cell\ viability\ (\%) = \frac{OD_{experimental\ group}}{OD_{control\ group}} \times 100\%$$

The IC_{50} value was determined using GraphPad Prism 6 software using the equation of log (inhibitor) vs response – variable slope.

Cell-cycle analysis

Cell-cycle analysis was performed to provide further explanation of the growth-inhibitory effect of liposomes. BGC-823 cells were seeded in 24-well plates at 1 × 10^5 cells/well. After treatment with free PTX, PTX-C-lipo, PTX-Rh2-lipo, PTX-Rg3-lipo, or PTX-Rg5-lipo (all 1 μg/mL PTX), Rh2-lipo, Rg3-lipo, Rg5-lipo, Rh2, Rg3, and Rg5 (equal concentration of each ginsenoside in all PTX-loaded ginsenoside liposomes) for 24 h, the cells were collected and fixed in ice-cold 75% ethanol at 4 °C overnight. The fixed cells were washed with PBS and stained with propidium iodide (PI) for 30 min. The amount of staining was then measured using flow cytometry (FACS Calibur; BD Biosciences).

Apoptosis assay

Apoptosis was detected using an Annexin V apoptosis detection kit, which monitors the translocation of phosphatidyl serine to the cell surface. The BGC-823 cells were digested and seeded in 24-well plates at 1 × 10^5 cells/well. After the cells were incubated with free PTX, PTX-C-lipo, PTX-Rh2-lipo, PTX-Rg3-lipo, and PTX-Rg5-lipo (all 10 μg/mL PTX), Rh2-lipo, Rg3-lipo, Rg5-lipo, Rh2, Rg3, and Rg5 (equal concentration of each ginsenoside in all PTX-loaded ginsenoside liposomes) for 48 h, apoptosis was measured by flow cytometry (FACS Calibur; BD Biosciences) to quantify the Annexin V-FITC/PI double staining. After treatment with PTX-C-lipo, PTX-Rh2-lipo, PTX-Rg3-lipo, and PTX-Rg5-lipo, apoptotic cells were labeled with PI (5 μg/mL) and Hoechst 33342 (5 μg/mL) and measured using a confocal microscope.

In vivo antitumor effect

The antitumor efficacy of PTX-loaded ginsenoside liposomes was evaluated by monitoring tumor growth in female nude mice (body weight: 18–20 g) xenografted with BGC-823 cells. When the tumor volume reached approximately 160 mm^3, the mice were randomly divided into six groups and injected via the tail vein with PBS, Lipusu®, Abraxane®, PTX-Rh2-lipo, PTX-Rg3-lipo, and PTX-Rg5-lipo (with a PTX dose of 10 mg/kg body weight) every 3 days for 21 days. The tumor size and body weight were measured every second day and

the tumor volume was calculated using the formula A × $B^2/2$, where A was the largest diameter and B was the smallest. The mice were anesthetized and sacrificed by cervical dislocation. The tumors were excised and weighed, and the organs were collected for histological examination.

Statistical analysis

Values are presented as the mean ± standard deviation (SD) and were analyzed using GraphPad Prism 6.0 software (GraphPad Software, CA, USA). Differences were assessed using one-way analysis of variance followed by the Newman-Keuls post-hoc test for multiple group comparisons and the Student's *t*-test for comparisons between two groups.

Results and Discussion

Characterization of ginsenoside liposomes

The ginsenoside liposomes were easily prepared following the procedures for the manufacture of conventional cholesterol liposomes. To be used as a nanocarrier for anticancer agents, appropriate particle size and uniform distribution of liposomes are required [38]. As shown in Figure 1B, the morphology of both the cholesterol and ginsenoside liposomes were spherical with a smooth surface; therefore, the incorporation of ginsenoside did not significantly alter the morphology of the liposomes. The mean particle sizes, PDIs, and ζ-potentials of the different formulations are shown in Table 1. Rh2-lipo and Rg3-lipo were approximately 50–60 nm, which was slightly smaller than C-lipo (80.13 ± 1.44 nm). However, the particle size of Rg5-lipo was large, being close to 100 nm. Notably, the ζ-potential of ginsenoside liposomes was much higher than that of C-lipo. Generally, a higher ζ-potential indicates better systemic stability. The higher ζ-potential and smaller size of ginsenoside liposomes may be related to the unique physicochemical properties of ginsenoside, which influence the order of lipid molecules and fluidity of the membranes. The stability of the liposomes was determined by evaluating the changes in their size over time. All liposomes were stable during the test period, with negligible changes in size and PDI (Figure 1C). However, the insertion of ginsenosides changed the size and surface status of liposomes, which might have altered the *in vivo* properties of liposomes to some extent [39].

To evaluate the effect of the incorporation of ginsenoside on the blood circulation of the liposomes, the three ginsenoside liposomes, C-lipo, and PEG-C-lipo were injected into the bloodstream of mice and the retention in the blood was evaluated over a period of 24 h. The period of circulation in the blood was longer for Rh2-lipo and Rg5-lipo than the others (Figure 1D); therefore, the elimination of Rh2-lipo and Rg5-lipo by the host was much slower. Moreover, the sustained circulation behavior of Rh2-lipo was similar to that of PEG-C-lipo. In contrast, Rg3-lipo did not exhibit a prolonged circulation time, which was similar to that found for C-lipo. The circulation behavior of the three ginsenoside liposomes was in the following order: Rh2-lipo > Rg5-lipo > Rg3-lipo. Thus, Rh2 and Rg5 have the potential not only to substitute for cholesterol as a membrane stabilizer, but to substitute for PEG to function as a stealth agent; thus, enhancing the passive targeting capacity of the liposomes. Importantly for a drug co-delivery system, longer blood circulation time not only improves the stability and prolongs the biological half-life of every component *in vivo*, but also specifically delivers the drugs to the tumor site via this enhanced permeability and retention effect [40].

Table 1. Characterization of blank liposomes and paclitaxel-loaded liposomes (n = 3; mean ± standard deviation).

	Size (nm)	PDI	ZP (mV)	EE (%)	LE (%)
C-lipo	80.13±1.44	0.23±0.005	-17.82±0.30		
Rh2-lipo	60.54±1.78	0.25±0.014	-37.21±1.49		
Rg3-lipo	52.02±1.42	0.11±0.002	-26.76±0.49		
Rg5-lipo	99.02±2.55	0.27±0.006	-31.36±1.46		
PTX-C-lipo	125.76±2.46	0.26±0.011	-21.86±0.82	90.1±1.6	6.4±0.2
PTX-Rh2-lipo	77.71±3.22	0.27±0.014	-39.21±1.03	91.3±2.1	5.6±0.3
PTX-Rg3-lipo	60.11±3.42	0.17±0.013	-29.32±0.41	95.5±3.3	7.3±0.4
PTX-Rg5-lipo	112.5±4.1	0.25±0.009	-34.4±0.8	82.8±1.6	4±0.1

Cellular uptake and internalization mechanism of ginsenoside liposomes

The GC targeting effect of ginsenoside liposomes was determined by examining the cellular uptake in BGC-823 cells. All three ginsenoside liposomes exhibited stronger green fluorescence signals inside BGC-823 cells than that of C-lipo (Figure 2A); therefore, ginsenoside modification effectively increased the uptake of liposomes by BGC-823 cells. Similarly, quantitative analysis of the cellular uptake showed that the fluorescence intensities of Rh2-lipo, Rg3-lipo, and Rg5-lipo in tumor cells were 3.1-, 2.5-, and 2.8-fold higher than that of C-lipo, respectively (Figure 2B and 2C).

To further investigate the possible internalization mechanism, the cellular uptake of ginsenoside liposomes was inhibited by various GLUT inhibitors, including D-glucose (blocking GLUT1), phloridzin (blocking SGLT1), and quercetin (blocking GLUT2 and GLUT5) [29, 35, 41, 42]. In the competition assay, at least one inhibitor exhibited significant inhibition of the internalization of each type of ginsenoside liposomes in the BGC-823 cells (Figure 2D–F, Figure S1A–C); therefore, the main

endocytic pathway of ginsenoside liposomes was GLUT carrier-mediated. Notably, the three ginsenosides increased the cellular uptake of liposomes via interaction with different GLUT carriers: Rh2-lipo mainly entered the cells through the GLUT1 pathway, Rg3-lipo was mainly taken up via the GLUT1 and SGLT1 pathways, and Rg5-lipo was mainly taken up by GLUT5 or GLUT2. Therefore, in addition to the passive targeting effect, ginsenoside liposomes accumulated in the tumor owing to active recognition and binding to the GLUT carriers on the tumor membrane. The GLUT inhibitors showed no effect with regard to C-lipo uptake (Figure S2).

In vivo tumor accumulation of ginsenoside liposomes

To further verify the *in vivo* GC targeting efficiency of ginsenoside liposomes, the real-time distribution of liposomes containing the same amount of DIR near-infrared dye was visualized (Figure S3). The fluorescence of the ginsenoside liposomes was distributed much more extensively in the tumor region at all time points compared to the C-lipo group (Figure 3A), revealing the excellent targeting ability of these liposomes. The efficient tumor-targeting capacity of ginsenoside liposomes was further verified by *ex vivo* imaging of the tumors, 24 h after injection. Intense fluorescence was observed in the tumors of all ginsenoside liposome-treated groups (Figures 3B and 3C). The targeting capacity of these different liposomes occurred in the following order: Rh2-lipo = Rg3-lipo > Rg5-lipo > C-lipo. Moreover, much weaker fluorescence signals were observed in the liver and spleen in the Rh2-lipo and Rg5-lipo groups, which corresponded to the slow clearance feature of these ginsenoside liposomes (Figure S4). Thus, the modification of ginsenoside Rh2 and Rg5 endowed the liposomes with dual functions to target

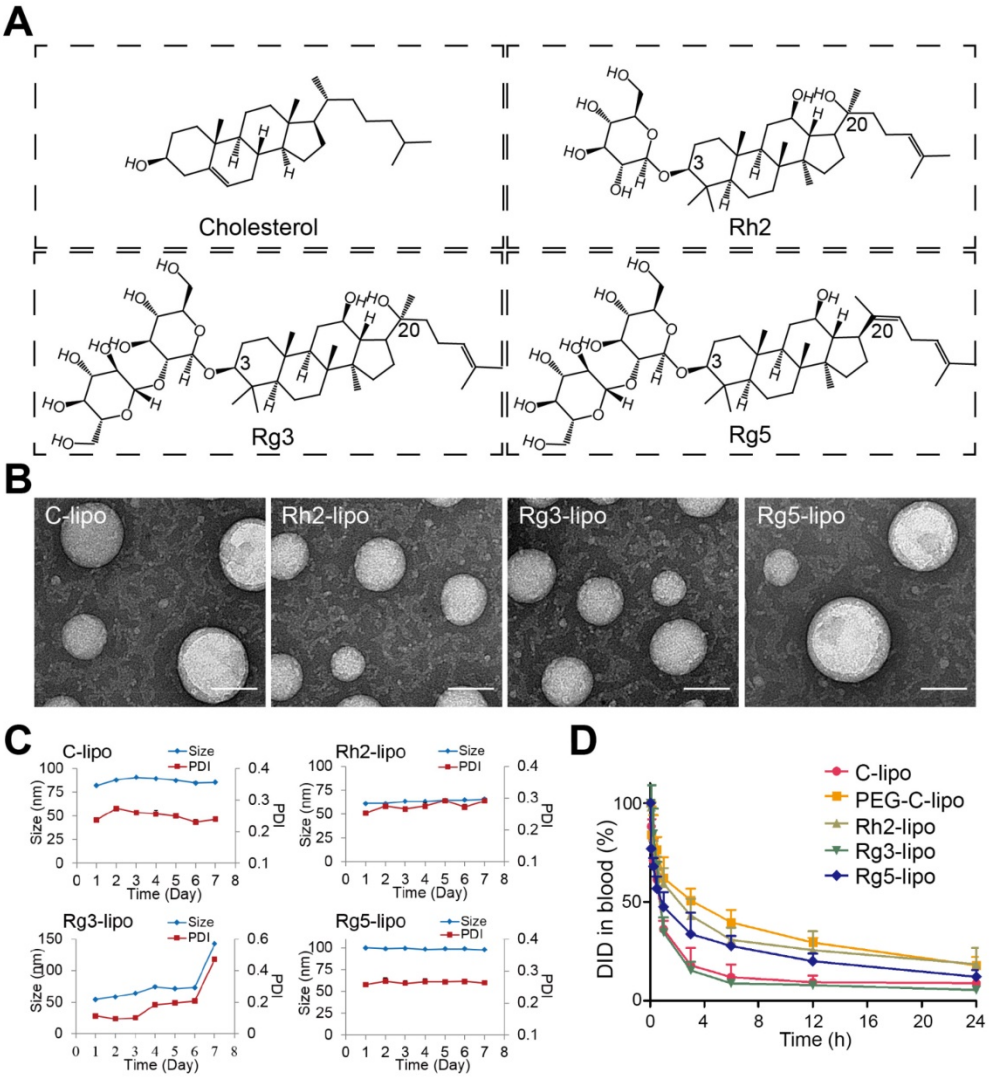

Figure 1. Characterization of ginsenoside liposomes. (A) Chemical structure of cholesterol and the ginsenosides. (B) Transmission electron microscope images of ginsenoside liposomes and cholesterol liposome (C-lipo); scale bar = 50 nm. (C) Change in size and polydispersity index of different liposomal formulations stored at 4 °C (n = 3; mean ± standard deviation [SD]). (D) Blood circulation profiles of C-lipo, polyethylene glycolated C-lipo (PEG-C-lipo), and three ginsenoside liposomes (n = 3; mean ± SD).

delivery to the tumor. First, the longer circulation time allowed the liposomes more time to utilize the passive targeting feature of the leaky tumor vasculature. Second, owing to the specific recognition of GLUT overexpression in GC, the liposomes were actively bound and internalized via GLUT-mediated endocytosis. However, although Rg3-lipo did not show any passive targeting effect, it still resulted in a stronger tumor-targeting effect than that of Rg5-lipo, which was due to its strong active targeting effect with GLUT on tumors.

Cytotoxicity of ginsenoside liposomes

To examine the antitumor activity of ginsenoside liposomes to GC, MTT, cell cycle, and apoptosis assays were performed on BGC-823 cells *in vitro*. First, the viability of BGC-823 cells was measured after treatment with free ginsenosides and ginsenoside liposomes. Free Rh2, Rg3, and Rg5 did not significantly inhibit the proliferation of BGC-823 cells, most likely due to the instability of free ginsenosides *in vitro* [13] (Figure 4A–C). When Rh2 and Rg3 were encapsulated in liposomes, their inhibition rates were substantially improved because of the increased stability and enhancement of the cellular uptake of free ginsenosides. Previous studies have shown that the IC_{50} values of ginsenoside Rg3 liposomes were significantly lower than those of free Rg3 on A549 and HepG-2 cells owing to the improved solubility and stability of Rg3 [43], although the formulation of ginsenoside liposomes was different to that used in the present study. Notably, the Rg5-lipo showed almost no toxicity to BGC-823 cells because of the weak toxicity of ginsenoside to this cell line. The toxicity of the three ginsenoside liposomes to BGC-823 cells occurred in the following order: Rh2-lipo > Rg3-lipo > Rg5-lipo (Figure 4D).

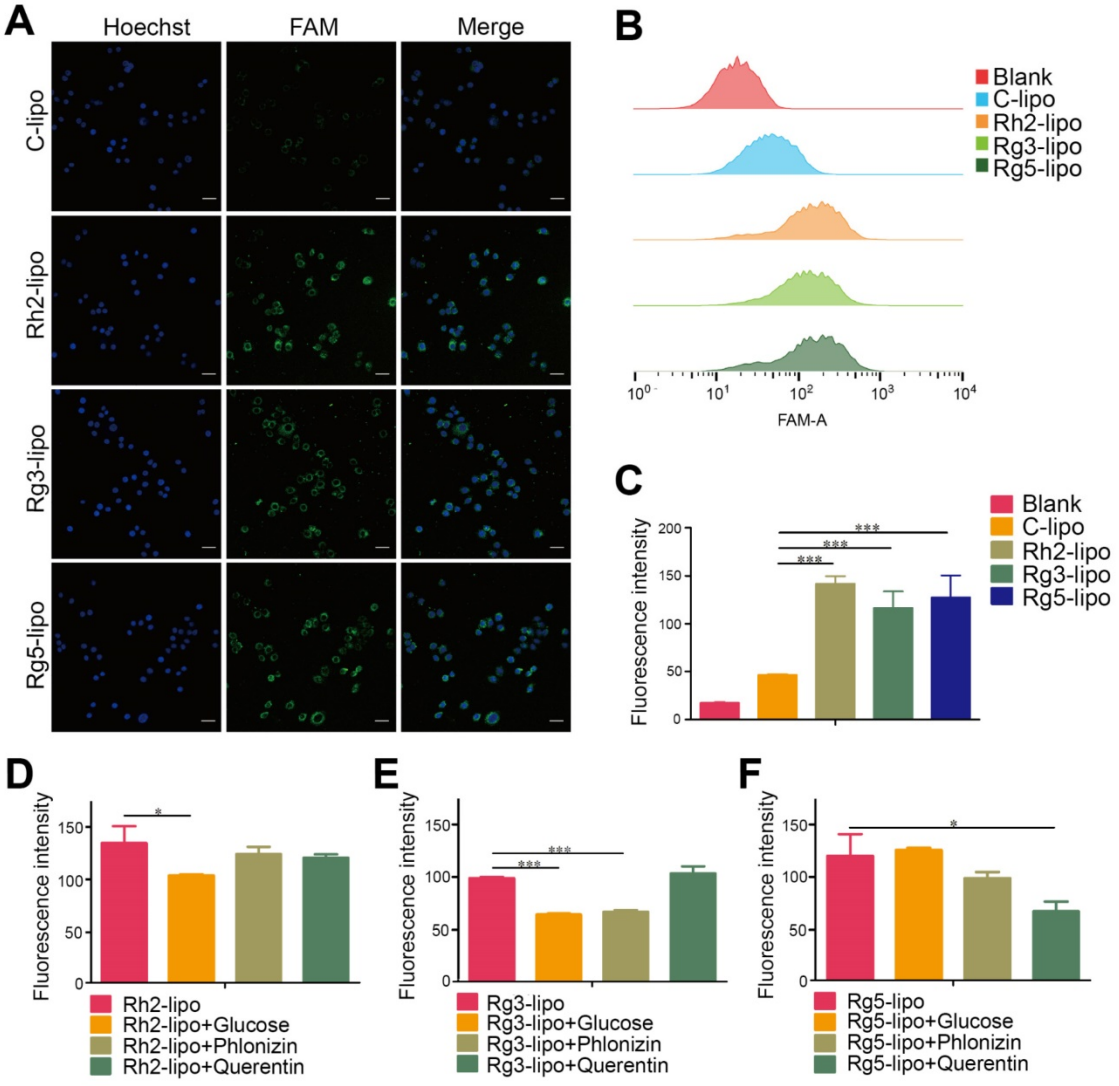

Figure 2. Cellular uptake and internalization mechanism of liposomes in BGC-823 cells. Qualitative (A) and quantitative (B and C) cellular uptake of carboxyfluorescein (FAM)-labeled liposomes in BGC-823 cells. The cells were incubated with 500 ng/mL FAM-loaded liposomes at 37 °C for 4 h (n = 3; mean ± standard deviation [SD]); scale bar = 50 μm. (D–F) Quantitative cellular uptake of ginsenoside liposomes with different glucose transporter inhibitors. The cells were pre-incubated with 20 mM glucose, 0.3 mM phloridzin, or 0.2 mM quercetin for 60 min, respectively (n = 3; mean ± SD). ***P < 0.001; *P < 0.05.

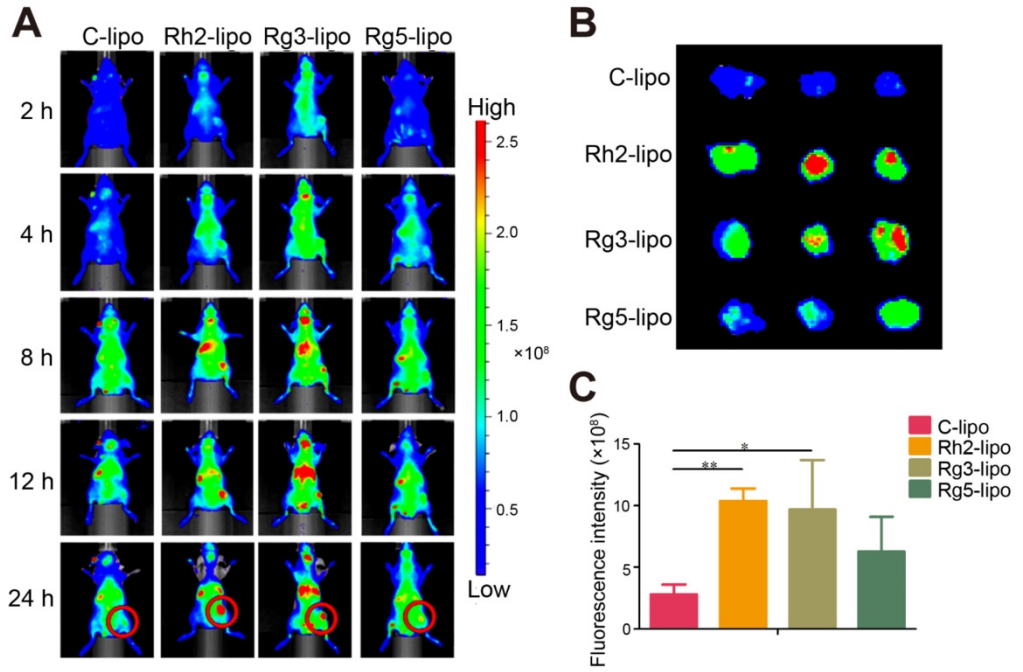

Figure 3. *In vivo* targeting effect of ginsenoside liposomes. (A) *In vivo* imaging of DiR-labeled C-lipo and ginsenoside liposomes in BGC-823 tumor-bearing mice. (B) *Ex vivo* imaging of excised tumors at 24 h after injection of DiR-labeled liposomes. (C) The relative fluorescence intensity in tumors from different groups (n = 3; mean ± standard deviation). *P < 0.05; **P < 0.01.

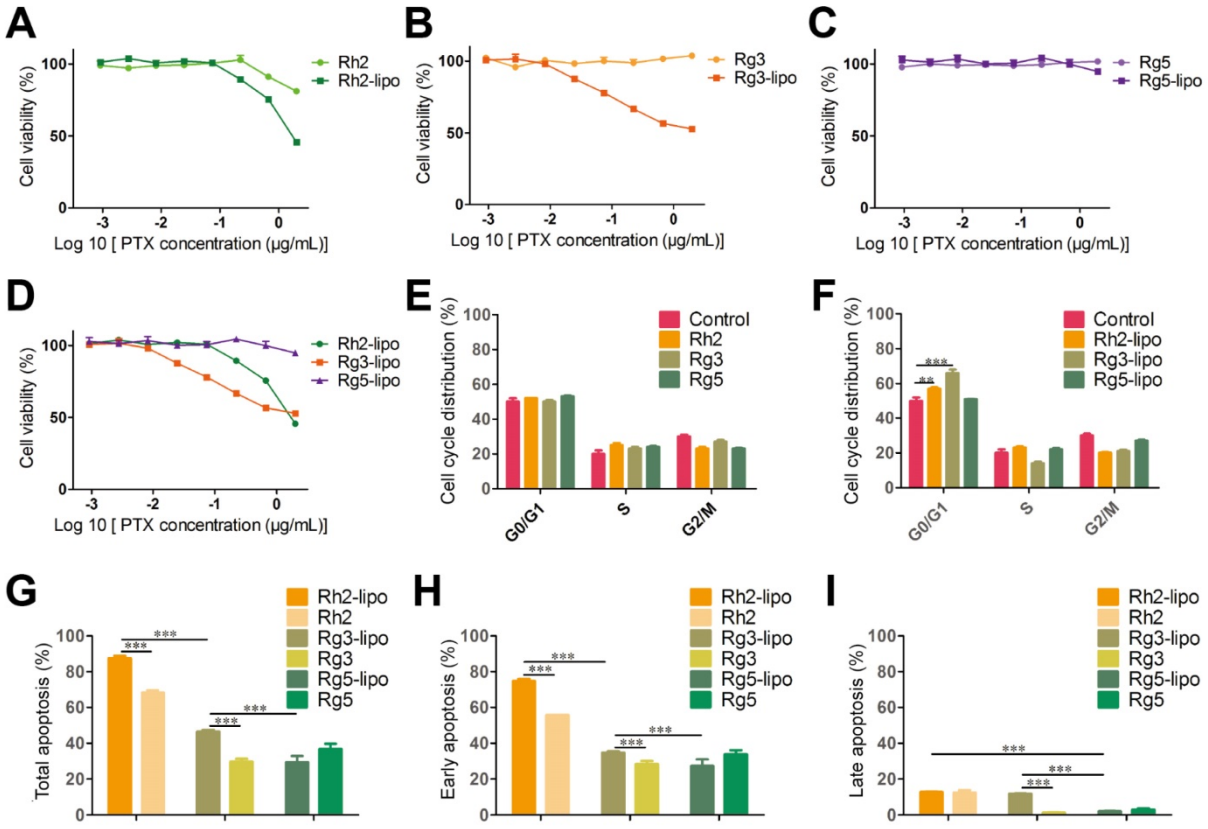

Figure 4. *In vitro* anticancer activities of ginsenoside liposomes. (A–E) Cytotoxicity of different ginsenoside liposomes and free ginsenosides to BGC-823 cells (n = 6; mean ± standard deviation [SD]). (E–F) Cell-cycle progression of BGC-823 cells treated with different ginsenoside liposomes and free ginsenosides (n = 3; mean ± SD). (G–I) Apoptosis induced by different ginsenoside liposomes and free ginsenosides in BGC-823 cells (n = 3; mean ± SD). **P < 0.01; ***P < 0.001.

The growth-inhibitory effect of liposomes can be further explained by alterations in the cell cycle. Studies have shown that Rh2, Rg3, and Rg5 can block the cell cycle in various cell types, including MCF-7, A549, and HeLa cells, during the G0/G1 phase [13]. However, the free ginsenosides tested in the present

study did not influence the BGC-823 cell cycle. In comparison, ginsenoside liposomes, especially Rh2-lipo and Rg3-lipo, significantly induced G0/G1 cell-cycle arrest (Figure 4E–F, Figure S5), with cell-cycle arrest not occurring unless the ginsenosides were encapsulated by the liposomes.

Apoptosis, the ultimate embodiment of antitumor effects, was evaluated using Annexin V-FITC/PI double staining. The percentage of total apoptotic cells showed that ginsenoside liposomes significantly promoted cellular apoptosis compared to free ginsenosides (Figure 4G). However, the apoptosis-inducing effects of Rg5-lipo were no different to those of its free form, which was consistent with previous results. The apoptosis-inducing effect of ginsenoside liposomes on BGC-823 cells were in the following order: Rh2-lipo > Rg3-lipo > Rg5-lipo. Ginsenosides mainly caused early apoptosis of tumor cells, rather than late apoptosis (Figure 4H–I, Figure S6). After the ginsenosides were encapsulated in liposomes, Rh2-lipo significantly increased the early apoptosis induced by Rh2, whereas Rg3-lipo enhanced both early and late apoptosis induction by free Rg3, and Rg5-lipo had no effect on either.

In vitro characterization of PTX-loaded ginsenoside liposomes

PTX was used as a model drug to ascertain the encapsulation capacity of ginsenosides as a membrane stabilizer. Ginsenoside liposomes readily formed small-size particles and PTX loading resulted in increased particle size, similar to other studies [44, 45]. The drug-loading effectiveness of various formulations is shown in Table 1, with no obvious differences observed. In addition, PTX-loaded liposomal formulations maintained a stable particle size and PDI when stored in PBS or 10% FBS (Figure S7A–C). However, significant differences were observed among the different formulations in the drug leakage test. PTX-Rh2-lipo and PTX-Rg3-lipo exhibited a steady behavior compared with the rapid drug leakage in PTX-C-lipo and PTX-Rg5-lipo whereby the cumulative leakage of PTX from the liposomes was less than 25% after 48 h (Figure S7D). Thus, Rh2-lipo and Rg3-lipo protected the drug from environmental damage. The cytotoxicity of PTX-loaded ginsenoside liposomes to BGC-823 cells is shown in Figure 5A–B. Compared with the relatively weak toxicity of ginsenoside liposomes, both free PTX and PTX-loaded liposomes significantly inhibited the proliferation of BGC-823 cells in a concentration-dependent manner, which confirmed the anticancer effect of PTX on GC. The IC_{50} values for ginsenoside liposomes were much lower than those for free PTX or PTX-C-lipo, indicating a stronger inhibitory effect by ginsenoside liposomes on this cell line. The excellent anticancer activity of PTX-loaded ginsenoside liposomes can be ascribed to the strong synergetic effect between ginsenoside and PTX, which was verified by the stronger cytotoxicity and lower IC_{50} value of PTX-loaded ginsenoside liposomes compared to the physical mixture of free PTX and blank ginsenoside liposomes (Figure S8). Similarly, the cell-cycle analysis showed that PTX played a major role in cell-cycle arrest during the G2/M phase, which was significantly magnified by the encapsulation of the drug in ginsenoside liposomes compared with that of C-lipo (Figure 5C, Figure S9).

The apoptosis assay showed that the total percentage of apoptotic cells induced by PTX-Rh2-lipo, PTX-Rg3-lipo, and PTX-Rg5-lipo was significantly higher than that induced by PTX-C-lipo and that induced by the corresponding blank ginsenoside liposomes (Figure 5D–E, Figure S10). Thus, ginsenosides function synergistically with PTX to induce tumor cell apoptosis. Furthermore, PTX-Rh2-lipo significantly promoted early apoptosis of tumor cells (early apoptosis rate of 85.83%), which correlated with the effect of Rh2-lipo (Figure 5F). However, unlike PTX-Rh2-lipo, PTX-Rg3-lipo and PTX-Rg5-lipo were more effective for the induction of late apoptosis, similar to the effects of free PTX and PTX-C-lipo. Therefore, in addition to the cooperation between the two ingredients, PTX and ginsenoside also have different apoptosis-inducing effects in the different formulations.

In summary, the results from the present study showed that the use of ginsenoside liposomes as a drug delivery agent could effectively combine the anticancer capabilities of chemotherapy agents and ginsenoside, and enabled ginsenoside and PTX to exert synergetic antitumor effects. The resulting cytotoxicity occurred in the following order: PTX-Rh2-lipo ≈ PTX-Rg5-lipo > PTX-Rg3-lipo. Therefore, in these formulations, ginsenoside functioned not only as the membrane material, but also as an adjuvant drug.

In vivo antitumor activity of PTX-loaded ginsenoside liposomes

To investigate the *in vivo* antitumor effects of the functionalized liposomes, mice with GC xenografts were treated with different PTX formulations. Two commercial PTX nanoformulations, Lipusu® and Abraxane®, were selected as to compare the efficiency of PTX-loaded ginsenoside liposomes against gastric carcinoma. Lipusu®, also known as Paclitaxel Liposome for Injection, is composed of PTX that is solubilized in liposome that has been formed from

lecithin and cholesterol, and is approved in China for clinical chemotherapy treatment. Abraxane®, the albumin-based formulation of PTX manufactured by Celgene, is currently recognized as the most effective and best-selling PTX formulation worldwide [46]. Abraxane® exhibited a modest growth-inhibitory effect on the BGC-823 tumor, whereas the antitumor effect of Lipusu® was not different to that of the PBS group at the end of the experiment (Figure 6A). However, all ginsenoside liposomes were much more effective than Abraxane® or Lipusu® for the inhibition of tumor growth. The tumor size and weight at the end of the experiment after the treatments with ginsenoside liposome were significantly decreased compared with that of the Abraxane® group, especially in the PTX-Rh2-lipo and PTX-Rg3-lipo groups where the tumors had almost disappeared (Figure 6B and 6C). PTX-Rg5-lipo was slightly inferior to the other two groups, which may be because of its weaker targeting effect. No decrease in body weight and discernible tissue damage was observed in any of the treatment groups (Figure 6D and 6E); therefore, no PTX-loaded ginsenoside liposome caused any off-target toxicity.

The outstanding antitumor activity of PTX-loaded ginsenoside liposomes can be ascribed three advantages: (1) a unique dual-function targeted drug delivery system; (2) an inherent antitumor effect of ginsenoside; (3) and a synergistic effect of the combination of ginsenoside and PTX against the tumor. The activity of the three PTX formulations against tumor growth was in the following order: PTX-Rh2-lipo ≈ PTX-Rg3-lipo > PTX-Rg5-lipo. PTX-Rh2-lipo and PTX-Rg3-lipo possessed all three advantages described above, whereas PTX-Rg5-lipo showed inferior targeting ability and was hampered by the weaker toxicity of Rg5-lipo, which contributed negatively to the antitumor performance.

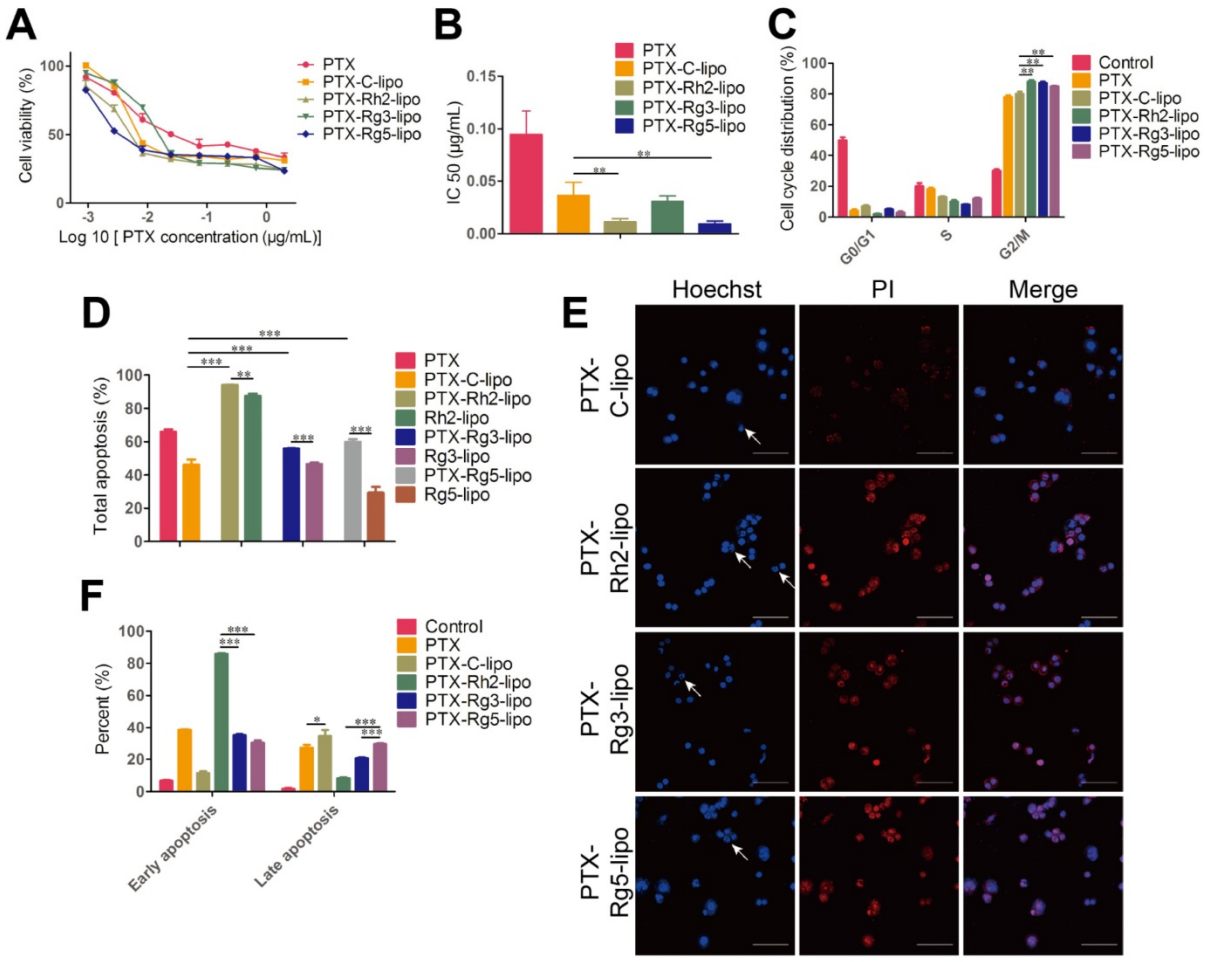

Figure 5. *In vitro* anticancer activities of paclitaxel (PTX)-loaded ginsenoside liposomes. Cytotoxicity (A) and IC_{50} values (B) of free PTX and different types of PTX-loaded liposomes in BGC-823 cells (n = 6; mean ± standard deviation [SD]). (C) Cell-cycle analysis of BGC-823 cells treated with free PTX and different types of PTX-loaded liposomes (n = 3; mean ± SD). (D, F) Induction of apoptosis by free PTX and different types of PTX-loaded liposomes in BGC-823 cells (n = 3; mean ± SD). (E) Inverted fluorescence microscope images of cell apoptosis (arrows indicate apoptotic bodies; scale bar = 100 μm). **P < 0.01; ***P < 0.001.

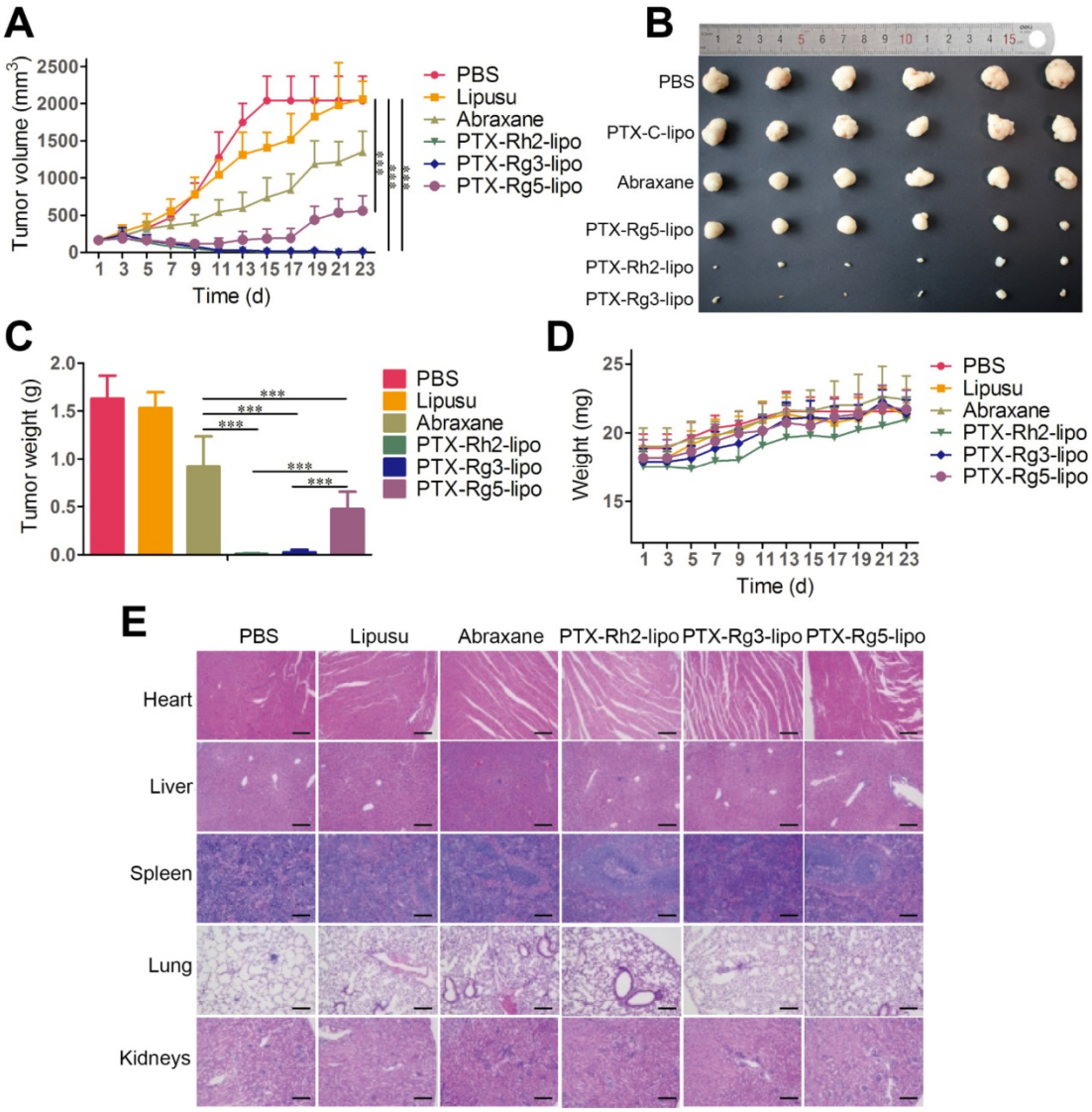

Figure 6. *In vivo* anticancer activities of paclitaxel (PTX)-loaded ginsenoside liposomes. (A) *In vivo* tumor growth inhibition after intravenous injection of different PTX formulations at a dose of 10 mg/kg (n = 6; mean ± SD). (B) Excised tumors from BGC-823 tumor-bearing nude mice on the day after the last injection (n = 6; mean ± SD). (C) Tumor weights of excised tumors (n = 6; mean ± SD). (D) Body weight variation over the course of the treatment (n = 6; mean ± SD). (E) Representative hematoxylin and eosin stained sections of the heart, liver, spleen, lungs, and kidneys (Scale bar = 100 μm). ***P < 0.001.

Conclusion

The major advantage of our approach is the simultaneous delivery of two agents with distinct action mechanisms to tumors. The combination of ginsenoside and PTX exhibited synergistic inhibition of the proliferation of human GC cells, which was caused by cell-cycle arrest and the induction of apoptosis. Controlling the delivery of drugs to the target site is essential so that the multiple free drugs can achieve the maximum anticancer effects of each of their individual components. Therefore, another advantage of our strategy lies in the development of a novel multifunctional liposome system, in which ginsenoside not only works as a chemotherapy adjuvant, but also as a membrane stabilizer that has long blood circulating time, and is an active targeting ligand. Unlike most drug carriers that are "torpid," ginsenoside liposomes exhibit multiple functionalities. We selected three ginsenosides with different structures as dual-use drug excipients to construct a unique nanocarrier and compared their functions, including blood circulation time, active recognition of GLUT, and tumor cytotoxicity. The combination therapy using drug-loaded ginsenoside liposomes yielded outstanding tumor growth suppression in a model of xenografted GC tumors and outperformed most reported PTX formulations, including Lipusu® and Abraxane®. The activity of the three PTX-loaded ginsenoside liposomes against tumor growth was in the following order: PTX-Rh2-lipo ≈ PTX-Rg3-lipo > PTX-Rg5-lipo. PTX-Rh2-lipo and PTX-Rg3-lipo showed outstanding tumor-targeting capacity and synergistic effects with

PTX, as well as exhibiting an inferior inherent antitumor effect. Nevertheless, PTX-Rg5-lipo was hampered by the weaker toxicity of Rg5-lipo, which contributed negatively to antitumor performance. This delivery system was versatile in the incorporation of anticancer agents with various structures and could be used as a simple preparation for the nanocarrier and the combination therapy protocol, thus simplifying clinical translation.

Abbreviations

C-lipo: cholesterol liposome; DID: 4-chlorobenzenesulfonate salt; DIR: 1,1′-dioctadecyl-3,3,3′,3′-tetramethylindotricarbocyanineiodide; DLS: dynamic light scattering; EE: encapsulation efficiency; EYPC: egg yolk lecithin; FAM: Carboxyfluorescein; GC: Gastric cancer; GLUT1: glucose transporter 1; LE: loading efficiency; MTT: 5-(dimethyl-thiazol-2-yl)-2,5-diphenyl-tetrazolium bromide; PDI: polydispersity index; PEG: polyethylene glycol; PTX: paclitaxel; Rh2-lipo: ginsenoside Rh2 liposomes; Rg3-lipo: ginsenoside Rg3 liposomes; Rg5-lipo: ginsenoside Rg5 liposomes; SGLT1: sodium-coupled glucose co-transporter 1.

Supplementary Material

Supplementary figures.
http://www.thno.org/v09p4437s1.pdf

Acknowledgements

We are thankful for financial support from the National Natural Science Foundation of China (No. 81773911, 81690263 and 81573616) and the Development Project of Shanghai Peak Disciplines-Integrated Medicine (No. 20180101).

Competing Interests

The authors have declared that no competing interest exists.

References

1. Yamamoto H, Watanabe Y, Maehata T, Morita R, Yoshida Y, Oikawa R, et al. An updated review of gastric cancer in the next-generation sequencing era: Insights from bench to bedside and vice versa. World J Gastroentero. 2014; 20: 3927-37.
2. Pozzo C, Barone C. Is there an optimal chemotherapy regimen for the treatment of advanced gastric cancer that will provide a platform for the introduction of new biological agents? Oncologist. 2008; 13: 794-806.
3. Layke JC, Lopez PP. Gastric cancer: Diagnosis and treatment options. Am Fam Physician. 2004; 69: 1133-40.
4. Barati N, Momtazi-Borojeni AA, Majeed M, Sahebkar A. Potential therapeutic effects of curcumin in gastric cancer. J Cell Physiol. 2019; 234: 2317-28.
5. Yeung KS, Gubili J, Mao JJ. Herb-Drug Interactions in Cancer Care. Oncology. 2018; 32: 516-20
6. Cheng YY, Hsieh CH, Tsai TH. Concurrent administration of anticancer chemotherapy drug and herbal medicine on the perspective of pharmacokinetics. J Food Drug Anal. 2018; 26: 88-95.
7. Ramos-Esquivel A, Viquez-Jaikel A, Fernandez C. Potential drug-drug and herb-drug interactions in patients with cancer: A prospective study of medication surveillance. J Oncol Pract. 2017; 13: 613-21.
8. Yu CP, Hsieh YC, Shia CS, Hsu PW, Chen JY, Hou YC, et al. Increased systemic exposure of methotrexate by a polyphenol-rich herb via modulation on efflux transporters multidrug resistance-associated protein 2 and breast cancer resistance protein. J Pharm Sci. 2016; 105: 343-9.
9. Ko CH, Yue GGL, Gao S, Luo KW, Siu WS, Shum WT, et al. Evaluation of the combined use of metronomic zoledronic acid and Coriolus versicolor in intratibial breast cancer mouse model. J Ethnopharmacol. 2017; 204: 77-85.
10. Sharma J, Goyal PK. Chemoprevention of chemical-induced skin cancer by Panax ginseng root extract. J Ginseng Res. 2015; 39: 265-73.
11. Park JY, Choi P, Kim T, Ko H, Kim H K, Kang KS, et al. Protective effects of processed ginseng and its active ginsenosides on cisplatin-induced nephrotoxicity: In vitro and in vivo studies. J Agric Food Chem. 2015; 63: 5964-9.
12. Pourmohamadi K, Ahmadzadeh A, Latifi M. Investigating the effects of oral ginseng on the cancer-related fatigue and quality of life in patients with non-metastatic cancer. Int J Hematol Oncol Stem Cell Res. 2018; 12: 313-7.
13. Wong AST, Che CM, Leung KW. Recent advances in ginseng as cancer therapeutics: a functional and mechanistic overview. Nat Prod Rep. 2015; 32: 256-72.
14. Zhou Y, Zheng X, Lu J, Chen W, Li X, Zhao L. Ginsenoside 20(S)-Rg3 inhibits the warburg effect via modulating DNMT3A/ MiR-532-3p/HK2 pathway in ovarian cancer cells. Cell Physiol Biochem. 2018; 45: 2548-59.
15. Zhang B, Zhou W, Gu CJ, Wu K, Yang HL, Mei J, et al. The ginsenoside PPD exerts anti-endometriosis effects by suppressing estrogen receptor-mediated inhibition of endometrial stromal cell autophagy and NK cell cytotoxicity. Cell Death Dis. 2018; 9: 574-87.
16. Wang Y, Xu H, Lu Z, Yu X, Lv C, Tian Y, et al. Pseudo-Ginsenoside Rh2 induces A549 cells apoptosis via the Ras/Raf/ERK/p53 pathway. Exp Ther Med. 2018; 15: 4916-24.
17. Liu Y, Fan D. Ginsenoside Rg5 induces apoptosis and autophagy via the inhibition of the PI3K/Akt pathway against breast cancer in a mouse model. Food Funct. 2018; 9: 5513-27.
18. Hou JG, Jeon BM, Yun YJ, Cui CH, Kim SC. Ginsenoside Rh2 ameliorates doxorubicin-induced senescence bystander effect in breast carcinoma cell MDA-MB-231 and normal epithelial cell MCF-10A. Int J Mol Sci. 2019; 20: 1244-59.
19. Wang J, Tian L, Khan MN, Zhang L, Chen Q, Zhao Y, et al. Ginsenoside Rg3 sensitizes hypoxic lung cancer cells to cisplatin via blocking of NF-kappaB mediated epithelial-mesenchymal transition and stemness. Cancer Lett. 2018; 415: 73-85.
20. Chen TL, Li BW, Qiu Y, Qiu ZD, Qu P. Functional mechanism of Ginsenosides on tumor growth and metastasis. Saudi J Biol Sci. 2018; 25: 917-22.
21. Chen ZJ, Cheng J, Huang YP, Han SL, Liu NX, Zhu GB, et al. Effect of adjuvant chemotherapy of ginsenoside Rg3 combined with mitomycin C and tegafur in advanced gastric cancer. Chin J Gastrointest Surg. 2007; 10: 64-6.
22. Boyko A, Alifirova V, Boyko O, Greshnova I, Zaslavskiy L, Zakharova M, et al. Pharmacokinetics and pharmacodynamics of PEGylated interferon beta-1a in patients with relapsing-remitting multiple sclerosis in the randomized double-blind placebo-controlled study. Mult Scler J. 2018; 24: 911-911.
23. Mi FL, Wang LF, Chu PY, Peng SL, Feng CL, Lai YJ, et al. Active tumor-targeted co-delivery of epigallocatechin gallate and doxorubicin in nanoparticles for combination gastric cancer therapy. Acs Biomater Sci Eng. 2018; 4: 2847-59.
24. Bulbake U, Doppalapudi S, Kommineni N, Khan W. Liposomal formulations in clinical use: an updated review. Pharmaceutics; 2017, 9: 12-45.
25. Akoev VR, Elemesov RE, Abdrasilov BS, Kim YA, Park HJ. Effects of triterpenoid glycosides of the dammaran series and their aglicons on phase transitions of dipalmitoylphosphatidylcholane. Biol Membrany. 1996; 13: 605-11.
26. Fukuda K, Utsumi H, Shoji J, Hamada A. Saponins can cause the agglutination of phospholipid-vesicles. Biochim Biophys Acta. 1985; 820: 199-206.
27. Noguchi Y, Marat D, Saito A, Yoshikawa T, Doi C, Fukuzawa K, et al. Expression of facilitative glucose transporters in gastric tumors. Hepato-Gastroenterol. 1999; 46: 2683-9.
28. Wang YZ, Xu Q, Wu W, Liu Y, Jiang Y, Cai QQ, et al. Brain transport profiles of ginsenoside Rb-1 by glucose transporter 1: In vitro and in vivo. Front Pharmacol. 2018; 9: 398-407.
29. Xiong J, Sun MJ, Guo JX, Huang LS, Wang SJ, Meng BY, et al. Active absorption of ginsenoside Rg1 in vitro and in vivo: the role of sodium-dependent glucose co-transporter 1. J Pharm Pharmacol. 2009; 61: 381-6.
30. Lv Q, Rong N, Liu LJ, Xu XL, Liu JT, Jin FX, et al. Antitumoral activity of (20R)- and (20S)-ginsenoside Rh2 on transplanted hepatocellular carcinoma in mice. Planta Med. 2016; 82: 705-11.
31. Chen JX, Peng HM, Xi OY, He XY. Research on the antitumor effect of ginsenoside Rg3 in B16 melanoma cells. Melanoma Res. 2008; 18: 322-9.
32. Quan K, Liu Q, Wan JY, Zhao YJ, Guo RZ, Alolga R, et al. Rapid preparation of rare ginsenosides by acid transformation and their structure-activity relationships against cancer cells. Sci Rep. 2015; 5: 8598-605.
33. Hong SS, Choi JY, Kim JO, Lee MK, Kim SH, Lim SJ. Development of paclitaxel-loaded liposomal nanocarrier stabilized by triglyceride incorporation. Int J Nanomed. 2016; 11: 4465-77.
34. Li RX, He YW, Zhu Y, Jiang LX, Zhang SY, Qin J, et al. Route to rheumatoid arthritis by macrophage-derived microvesicle-coated nanoparticles. Nano Lett. 2019; 19: 124-34.
35. Guo YB, Zhang YJ, Li JF, Zhang Y, Lu YF, Jiang XT, et al. Cell microenvironment-controlled antitumor drug releasing-nanomicelles for

GLUT1-targeting hepatocellular carcinoma therapy. Acs Appl Mater Inter. 2015; 7: 5444-53.
36. Xu H, Liu XY, Yang JN, Liu R, Li TL, Shi YL, et al. Cyanine-based 1-amino-1-deoxyglucose as fluorescent probes for glucose transporter mediated bioimaging. Biochem Bioph Res Co. 2016; 474: 240-6.
37. Jiang XY, Xin HL, Ren QY, Gu JJ, Zhu LJ, Du FY, et al. Nanoparticles of 2-deoxy-D-glucose functionalized poly(ethylene glycol)-co-poly(trimethylene carbonate) for dual-targeted drug delivery in glioma treatment. Biomaterials. 2014; 35: 518-29.
38. Chen CT, Duan ZQ, Yuan Y, Li RX, Pang L, Liang JM, et al. Peptide-22 and cyclic RGD functionalized liposomes for glioma targeting drug delivery overcoming BBB and BBTB. Acs Appl Mater Inter. 2017; 9: 5864-73.
39. Senior J, Delgado C, Fisher D, Tilcock C, Gregoriadis G. Influence of surface hydrophilicity of liposomes on their interaction with plasma-protein and clearance from the circulation - studies with poly(ethylene glycol)-coated vesicles. Biochim Biophys Acta. 1991; 1062: 77-82.
40. Nakamura Y, Mochida A, Choyke PL, Kobayashi H. Nanodrug delivery: Is the enhanced permeability and retention effect sufficient for curing cancer? Bioconjugate Chem. 2016; 27: 2225-38.
41. Gauer JS, Tumova S, Lippiat JD, Kerimi A, Williamson G. Differential patterns of inhibition of the sugar transporters GLUT2, GLUT5 and GLUT7 by flavonoids. Biochem Pharmacol. 2018; 152: 11-20.
42. Andrade N, Araujo JR, Correia-Branco A, Carletti JV, Martel F. Effect of dietary polyphenols on fructose uptake by human intestinal epithelial (Caco-2) cells. J Funct Foods. 2017; 36: 429-39.
43. Yu H, Teng LR, Meng QF, Li YH, Sun XC, Lu JH, Lee RJ, et al. Development of liposomal Ginsenoside Rg3: Formulation optimization and evaluation of its anticancer effects. Int J Pharmaceut. 2013; 450: 250-8.
44. Jain S, Kumar D, Swarnakar NK, Thanki K. Polyelectrolyte stabilized multilayered liposomes for oral delivery of paclitaxel. Biomaterials. 2012; 33: 6758-68.
45. Chen YC, Xia R, Huang YX, Zhao WC, Li J, Zhang XL, et al. An immunostimulatory dual-functional nanocarrier that improves cancer immunochemotherapy. Nat Commun. 2016; 7: 13443-55.
46. Sofias AM, Dunne M, Storm G, Allen C. The battle of "nano" paclitaxel. Adv Drug Deliver Rev. 2017; 122: 20-30.